applied sciences

MDPI

Article

A Theoretical Proposal for an Actively Controlled Ultra-Wideband Absorber Based on Vanadium Dioxide Hybrid Metamaterials

Ubaid Ur Rahman Qureshi [1], Muhammad Ismail Khan [2] and Bin Hu [1,*]

[1] School of Optics and Photonics, Beijing Institute of Technology, Beijing 100081, China
[2] Department of Electrical Engineering, COMSATS University Islamabad, Abbottabad 22060, Pakistan
* Correspondence: hubin@bit.edu.cn

Abstract: In this study, an ultra-wideband actively tunable terahertz absorber composed of four identical arc-shaped structures made of phase transition material vanadium dioxide (VO_2) is presented. A metal ground plane is placed at the bottom and an insulating spacer (quartz) as the middle dielectric layer. Simulation results demonstrate 90% absorption with a broad bandwidth spanning 3 THz (2.7 THz–5.7 THz) under normal incidence. The proposed structure transforms from a reflector to an absorber by changing the conductivity from 200 S/m to 2×10^5 S/m; the absorbance at peak frequencies can be consistently tuned from 4% to 100%. Absorption spectra demonstrate that the polarization angle does not affect the response of the proposed structure. Power loss density (PLD) and impedance-matching theory are further analyzed to learn more about the physical origin of ultra-wide absorption. The ultra-wide operating bandwidth, high absorption efficiency, active tunability, and independence of polarization make the proposed structure an excellent candidate for integration into profound THz applications such as sensors, modulators, and optic-electro switches.

Keywords: ultra-wideband; terahertz; absorption spectra

Citation: Qureshi, U.U.R.; Khan, M.I.; Hu, B. A Theoretical Proposal for an Actively Controlled Ultra-Wideband Absorber Based on Vanadium Dioxide Hybrid Metamaterials. *Appl. Sci.* **2022**, *12*, 10164. https://doi.org/10.3390/app121910164

Academic Editor: Dimitrios Zografopoulos

Received: 11 September 2022
Accepted: 6 October 2022
Published: 10 October 2022

1. Introduction

In recent years, terahertz (THz) waves gained popularity due to their applications in wireless communication, sensing, and imaging. [1–4]. To meet the challenges posed by the emerging THz applications, several metamaterial-based devices were suggested, including filters [5–7], absorbers [8–10], polarity converters [11], and others. Metamaterial perfect absorbers are one of these valuable gadgets that play a central role in many THz applications such as emitters of heat [12,13], solar-powered cells [14,15], and stealth technology [16,17]. Therefore, realizing ultra-wideband efficient absorbers has always been of profound interest to the research community and industry. In this regard, studies in the literature suggested multi-band, dual-band, and narrow-band absorbers [18–21]. Aside from a specific absorption bandwidth, these metamaterial perfect absorbers (MPAs) are inflexible in their electromagnetic responses. It is demonstrated that different sized resonant structures in a single unit cell can be used to produce broadband absorption [22–24]. Another alternative is a multilayer construction with different thickness dielectric layers [25–27]. However, MPAs made with the earlier methods are difficult to realize and control [28–31]. Several progress reports integrate metamaterials with semiconductors, graphene, and liquids crystals, while others use phase transition materials [28–30] to achieve active control.

The insulating material can be transformed into metallic by using electrical, thermal, or optical stimuli, such as UV light. The rapid reaction time and wide modulation depth of VO_2 make it more suitable for integrating into tunable absorbing structures. Various VO_2-based absorbers with broadband and adjustable absorption capabilities were recently discovered. Several studies demonstrate that electrical [32–34], thermal [35,36], or optical excitation [37,38] can induce the phase shift. Using metamaterials with VO_2 seems to be a potential approach to achieving THz re-configurability [39–50]. The electrical conductivity of vanadium dioxide (VO_2), a phase transition material, can alter by several magnitudes as the material goes through its phase transition [51,52]. In this regard, a tunable broadband terahertz absorber constructed of four identical vanadium dioxide (VO2) square loops with a 2.45 THz absorption bandwidth is presented in [53] under normal incidence. A quatrefoil and circle-loaded complementary square split ring resonator (CSSRR) are presented in [54], which show two peaks at 0.88 and 1.42 THz. The in-plane and out-of-plane components of its surface susceptibility tensor can be reliably determined with the optical detection of the susceptibility tensor in two-dimensional crystals, as presented in [55]. Table 1 has summarized MPAs with broadband and adjustable VO_2 absorption properties (see [39–45,52–54] in Table 1).

Table 1. Comparison table of the absorption capabilities of various VO_2-based absorbers.

References	Absorption Bandwidth (THz)	Absorptance	Tunable Range (%)	Material
[39]	0.34	>90%	30–100	VO_2
[40]	0.66	>90%	30–98	VO_2
[41]	0.53	>90%	5–100	VO_2
[42]	1.24	>90%	15–96	VO_2
[43]	0.56	>90%	9–99.3	VO_2 and graphene
[44]	1.24	>90%	5–100	VO_2
[45]	0.89, 0.78	>80%	20–90 44–85	VO_2
[52]	1.79	>90%	20–99	VO_2 and graphene
[53]	2.45	>90%	4–100	VO_2
[54]	1.07	>90%	20–100	VO_2
Proposed work	**5.7 − 2.7 = 3**	**>90%**	**4–100**	**VO_2**

This paper proposes a tunable ultra-wideband absorber composed of a three-layer (VO_2/quartz/Au) configuration. The absorber achieves excellent absorption of approximately 90% in the range of 2.7 THz–5.7 THz. The absorptivity of this absorber varies between 4% and 100% with the changing conductivity of VO_2. According to the comparative Table 1, the absorber performs much better than the other VO_2-based absorbers in terms of operating band and efficiency. Power loss density and impedance-matching theory are applied to elaborate on the physical origin of ultra-wide absorption.

2. Design Methodology

The geometrical structure of the ultra-wideband THz absorber is shown in Figure 1a. It consists of three layers; a VO_2 arc-shaped patch on the top, a metal ground plane of gold (Au) placed at the bottom, and an insulating spacer (quartz) as the middle dielectric layer. The final optimized geometrical parameters are determined as a result of parametric scanning. p = 75 µm, t = 0.2 µm, h = 11 µm, s1 = s2 = 17 µm, c = 1 µm, b = 5 µm a = w1 = 4 µm, w = 23 µm, and L = 17 µm. The thickness of the top layer VO_2 is 0.2 µm. In our simulations, we used a quartz substrate with a permittivity of 2.25 [46]. The conductivity of gold (Au) is $\sigma = 5.8 \times 10^7$ S/m. The optical properties of VO_2 in the THz range [34–37] are described using the Drude model, which may be stated as:

$$\varepsilon(\omega) = \varepsilon_\infty - \frac{\omega_p^2(\sigma)}{\omega^2 + i\, r\omega}$$

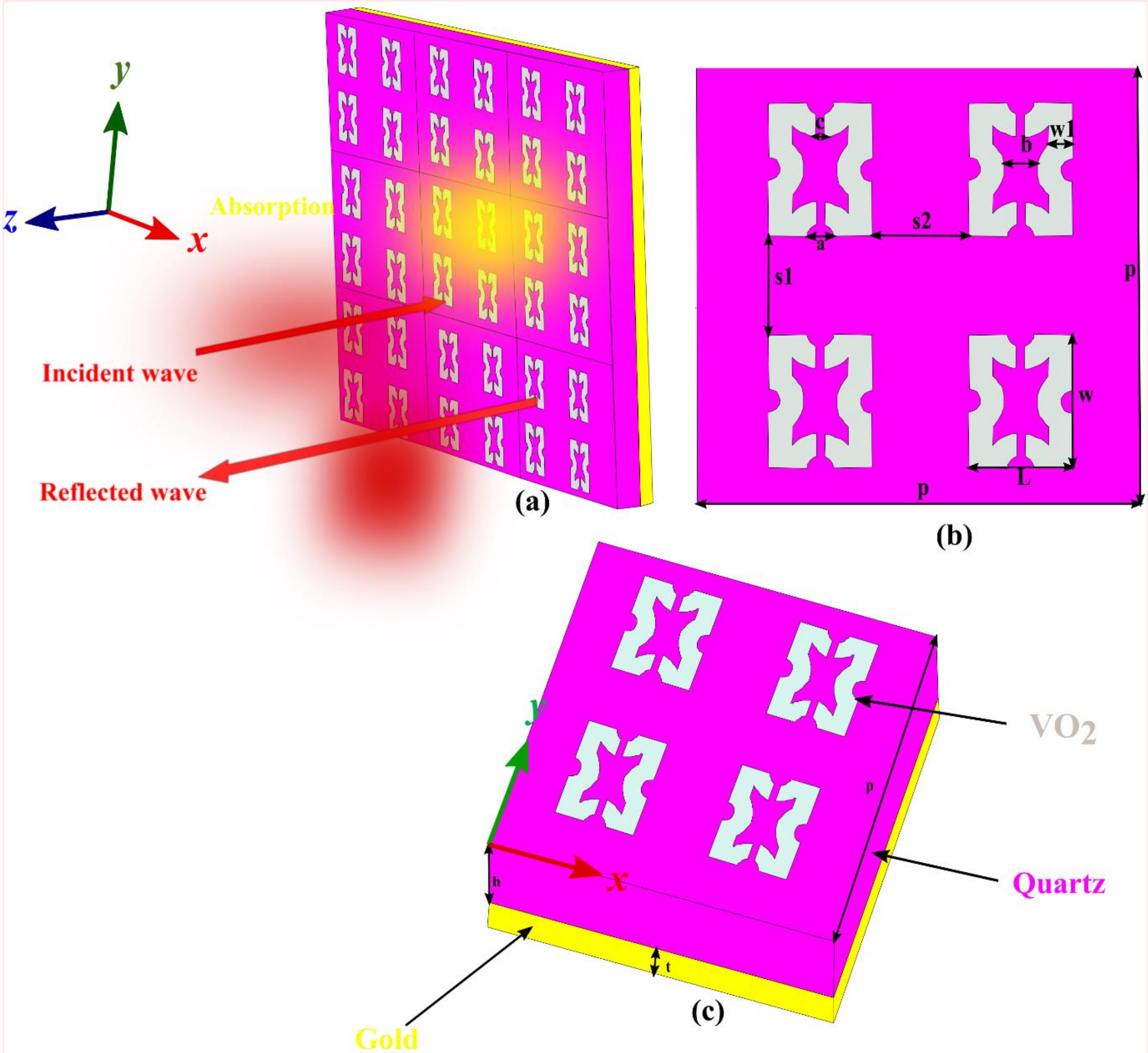

Figure 1. (**a**) 3 × 3 array of the design metasurface; (**b**) the top view of the schematic unit cell; (**c**) three-dimensional view of the proposed planar ultra-wideband unit cell absorber.

The permittivity at infinite frequency is represented by $\varepsilon_\infty = 12$. The collision frequency (γ) is 5.75×10^{13} rad/s, while the plasma frequency, $\omega_\rho(\sigma_0)$, depends on conductivity. As a function of σ, plasma frequency $\omega_\rho(\sigma)$ can be represented as:

$$\omega_{P^2}(\sigma) = \frac{\sigma}{\sigma_0}\,\omega_P^2\,\sigma_0$$

with $\sigma = 3 \times 10^5$ S/m and $\omega_\rho(\sigma_0) = 1.4 \times 10^{15}$ rad/s.

In this work, thermally, VO_2 changes from an insulator to a metal state, with conductivity increasing from 200 S/m to 2×10^5 S/m. At approximately 340 K, it is known that VO_2 can undergo a phase shift from insulator to metal [54]. CST Microwave Studio was used to simulate the electromagnetic response of the proposed absorber over the frequency range of 2–7 THz. The simulation employs a configuration for adaptive tetrahedron mesh refinement. To model an infinite array, periodic boundary conditions ire used with an electric field (E-field) along the *x*-axis and a magnetic field (H-field) along the *y*-axis. To incident a linearly polarized wave, floquet ports are used along the *z*-axis.

The absorption is computed as follows as $A(\omega) = 1 - R(\omega) - T(\omega)$, where $R(\omega) = |S_{11}|^2$ and $T(\omega) = |S_{21}|^2$. S_{11} and S_{21} are numerically calculated reflection and transmission coefficients. Since the thickness of the back metallic layer (Au = 0.2 μm) is much larger than the skin depth, the transmittance T(ω) is close to 0, as shown in Figure 2 (T(ω) = S21 = 0). As a result, the absorptivity is as follows:

$$A(\omega) = 1 - R(\omega)$$

Therefore, the concept of impedance-matching theory achieves a highly efficient broadband absorption from a range of 2.7 to 5.7 THz.

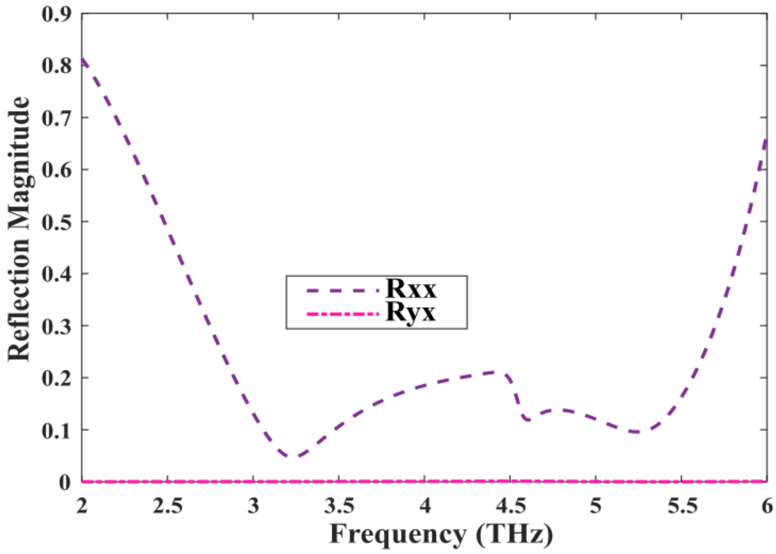

Figure 2. Magnitude of reflection coefficients of the design structure when conductivity of metal is $\sigma = 2 \times 10^5$ S/m.

3. Simulation Results and Discussion

Even though the incident field consists of a single component, the reflected field typically has both x and y components. The co-polarized reflection coefficients are defined as $R_{xx} = |Erx|/|Eix|$ and the cross-polarized reflection coefficients as $Ryx = |Ery|/|Eix|$ when the incident and reflected fields are x and y polarized, respectively. The simulated results of the proposed design for linear reflection coefficient (R_{xx} and R_{yx}) under normal incidence are shown in Figure 2. It can be seen from Figure 2 that the cross-polarized reflection coefficient (R_{yx}) is equal to zero in the interested band when the top layer of VO_2 is in the metal state, while the co-polarization reflection coefficient is almost equal to 0.1 in the frequency range of 2.7–5.7 THz. Therefore, the proposed design achieves perfect absorption in the frequency range of 2.7–5.7 THz as shown in Figure 3. Figure 3a displays the absorber's reflection and absorption spectrum when the top layer of VO_2 is in the metal state. The result shows that the designed absorber achieves more than 90% in the frequency range of 2.7–5.7 THz at a normal incidence angle. For most of the operating band, absorption efficiency exceeds 98%. The absorber features four absorption peaks at resonance frequencies: 3.2 THz, 3.8 THz, 4.7 THz, and 5.2 THz. In practical applications, the impact of wave polarization and incident angle on absorption efficiency must be considered. When electromagnetic radiation is incident vertically, the VO_2 metal phase's absorption spectra are displayed in Figure 3b at various polarization angles. The proposed absorber's absorption spectra are unaffected by polarization angles between 0° and 45°. As a result, the absorption is indifferent to the polarization angle. This polarization independence is essential in absorbers because the polarization angle is frequently random under actual settings. In order to dynamically control the absorption of the schematic design absorber, the conductivity of arc-shaped VO_2 varies as the intrinsic structure of VO_2 allows it to make the transition from the insulating to the metallic state. Numerical simulations are performed in order to see the effects of variations in the conductivity of

VO_2 on the absorption efficiency. As shown in Figure 3, absorption efficiency increases with increase in the conductivity. The design absorber achieves a perfect absorption of more than 90% in the frequency range of 2.7–5.7 THz, resulting in an absorption bandwidth of up to 3 THz. The optical absorption spectra show that by raising the conductivity from 200 to 20 $\times$ 10^4 S/m, the absorption at resonant frequencies may be continuously tuned from 4% to 100%, with the associated absorptance frequency band reaching 3 THz.

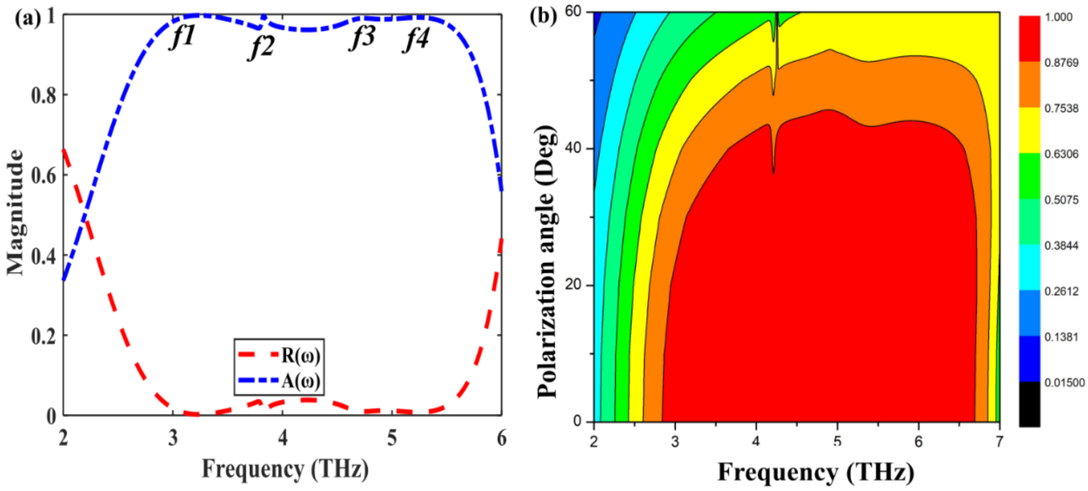

Figure 3. (**a**) Ultra-wideband absorber reflection and absorption spectra. (**b**) Polarization angle color absorption spectrum map.

Figure 4a shows the absorber's magnitude reflection and absorption spectra when the VO_2 material is in the metal phase. The absorber has four resonance peaks at 3.2 THz, 3.8 THz, 4.7 THz, and 5.2 THz. The results reveal that absorption efficiency is greater than 90% in the range 2.7 THz–5.7 THz on a normal incidence angle. Absorption efficiency surpasses 98% for the majority of the working spectrum. When conductivity changes, the changes in the imaginary parts are far more significant than those in the real parts, as shown in Figure 5. As a result, the spectral intensity shifts substantially, but the peak's placement along the frequency axis remains virtually unchanged. Figure 6 shows that at conductivities of 1.5 $\times$ 10^5 S/m, 100% absorption spectra in the frequency range of 3.38–5.19 THz is achieved.

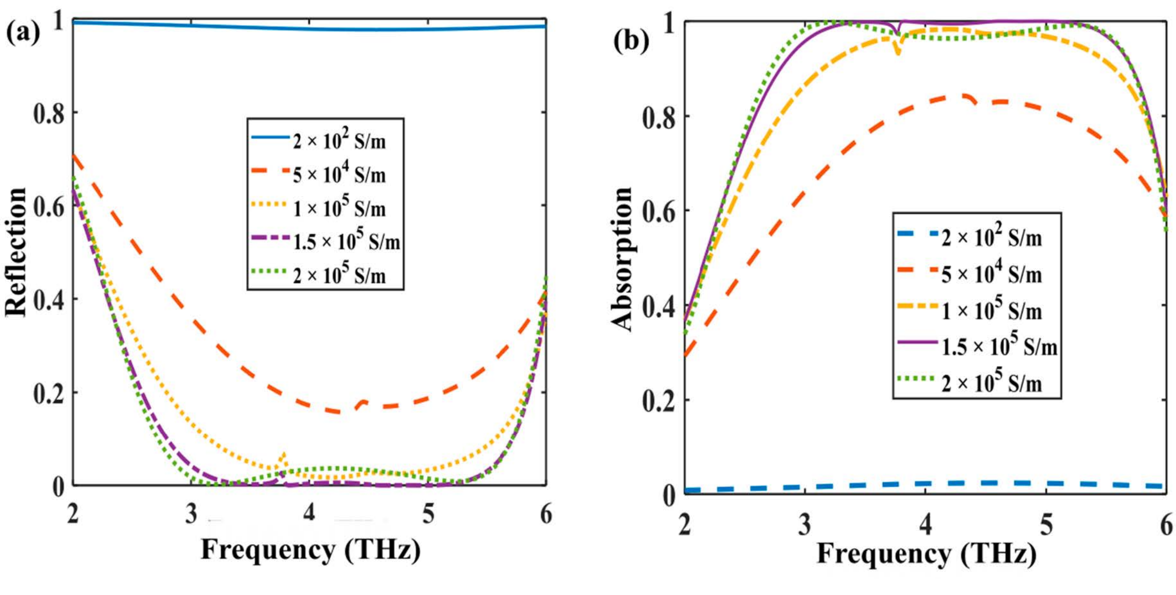

Figure 4. (**a**) Numerical reflection spectra and (**b**) absorption spectra of VO_2 at various conductivities.

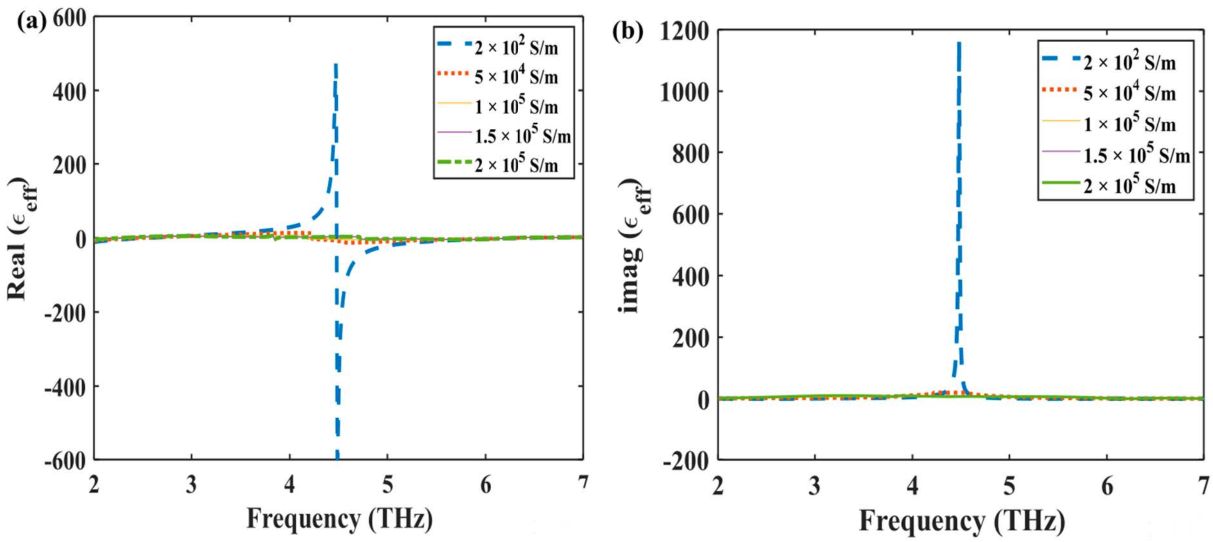

Figure 5. (**a**) The real part of the effective permittivity and (**b**) imaginary parts of effective permittivity for varying VO_2 conductivities.

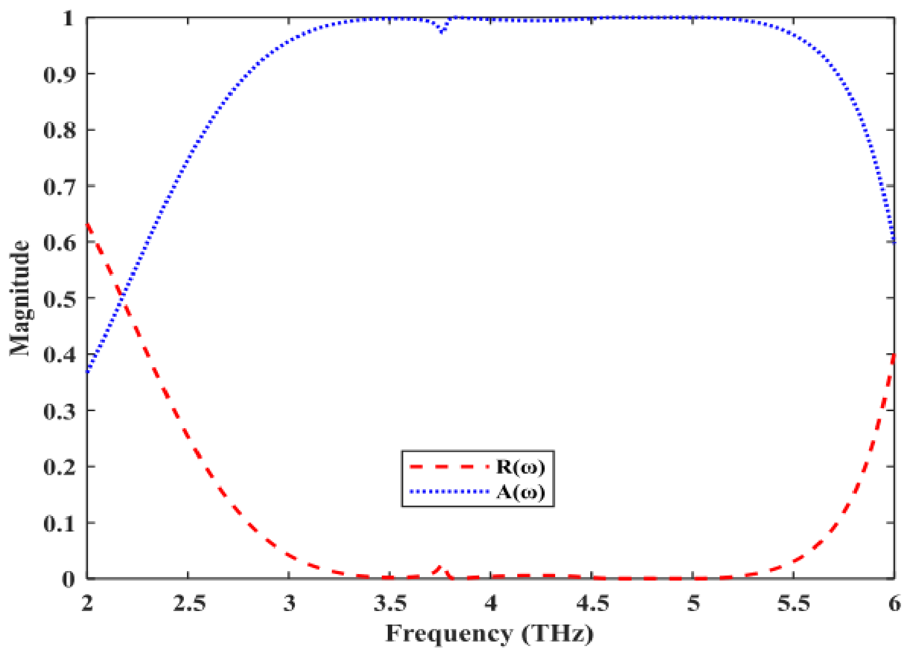

Figure 6. The absorption spectra of the design structure at 1.5×10^5 S/m VO_2 conductivities.

4. Calculation of Retrieved Effective Physical Parameters

To explain the perfect absorption properties and tunable mechanism, the impedance theory is applied to determine the retrieved effective physical parameters from Equations (1)–(4) of the design structure. CST (MICROWAVE STUDIO) is used to extract the S-parameters. Compared to the Drude–Lorentz approach, S-parameters for complex structures yield more accurate permittivity and permeability values [49]. It is possible to write the system's S-parameters [50]. Figure 1 depicts the schematic metasurface with a typically incident plane wave.

$$S_{11} = \frac{R_{01}\left(1 - e^{i2nk_0d}\right)}{1 - R_{01}^2 e^{i2nk_0d}} \tag{1}$$

$$S_{21} = \frac{\left(1 - R_{01}^2\right)e^{i2nk_0d}}{1 - R_{01}^2 e^{i2nk_0d}} \tag{2}$$

Solving Equations (1) and (2) gives impedance (Z)

$$= \pm\sqrt{\frac{(1+s_{11})^2 - s_{21}^2}{(1-s_{11})^2 - s_{21}^2}} \tag{3}$$

$$e^{i2nk_0d} = \frac{S_{21}}{1 - S_{11}\frac{z-1}{z+1}} \tag{4}$$

$$n = \frac{1}{K_0 d}\left[\{[ln(e^{ink_0d})]'' + 2m\pi\} - i[ln(e^{ink_0d})]'\right] \tag{5}$$

where $(.)''$ represent the complex element and $(o)'$ represent real part of complex number. The refractive index is denoted by n; z = impedance; k_0 = wavenumber; d = maximum unit element length; k_0 = wavenumber; m = branch due to sinusoidal periodicity, and electric and magnetic field components are denoted by E and H, respectively. The following expressions link effective physical parameters with each other:

$$\varepsilon_{effective} = \frac{n}{z} \tag{6}$$

$$\mu_{\mathrm{effective}} = nz \tag{7}$$

Figure 7 shows the effective physical characteristics for perfect absorption when $\sigma = 2 \times 10^5$ S/m. The proposed absorber exhibits a negative refractive index and a positive impedance, indicating that the hypothesized metasurface behavior is in the band of interest. It can be seen from Figure 7a that in the 4 THz–5.7 THz frequency band, permittivity is negative. Figure 7 also presents the proposed THz absorber's refractive index and impedance. Complete absorption can occur when the absorber's effective impedance is equal to the free space impedance (377 Ohm). The fundamental electromagnetic theory demonstrates that the surface reflection is reduced to zero when a structure's effective permeability and permittivity are equal to those of free space. Figure 8 shows the relative impedance of the proposed absorber for different VO_2 conductivities. For VO_2 with a conductivity of 2×10^5 S/m, the real part of the impedance is close to 1 (equivalent to free space) in the frequency range of 2.7–5.7 THz, while the imaginary parts are close to zero. Consequently, the parametrically optimized geometry of the metasurface's impedance is equal to that of free space. It satisfies the strategy requirements for a perfect absorber.

To realize THz absorption, we start with a single VO_2 arc-shaped rectangle, which is placed on top of a quartz substrate to form a conventional metamaterial perfect absorber (MPAs) unit cell structure, as shown in Figure 9a, while in Figure 10a, the relative impedance is mismatched, and, due to this, there is no absorption. When the number of arc-shaped VO_2 patches increases on the top of the quartz substrate, the absorption bandwidth increases because the impedance becomes closer to that of the free space, as shown in Figure 10b,c. In the case of four identical arc-shaped VO_2 patches, the absorption efficiency and bandwidth increase, as seen in Figures 9d and 10d, respectively. We carried out a numerical simulation analysis of the power loss density (PLD) to better understand the physical workings of the designed metasurface. PLD is measured in W/m^3 and indicates the material's electric power density. PLD distribution evolution at different peak absorption bands (*f1*, *f2*, *f3*, *f4*) when $\sigma = 2 \times 10^5$ m/s (metal phase) is shown in Figure 11a–d. At the absorption bands of 3.2 THz, 4.7 THz, and 5.2 THz, energy is only focused on arc-shaped VO_2 patterns. In comparison, at 3.7 THz, power is concentrated above the VO_2 structure and at the blank middle dielectric layer (Figure 11b). The arc-shaped VO_2 structure and the middle dielectric layer show large PLD distribution due to contact between nearby unit cells. When the VO_2 structure is in the insulator state at $\sigma = 100$ m/s, the PLD is low, showing the structure's non-resonant response. The energy dissipation is non-local, in contrast to Figure 11a–d, demonstrating that VO_2 can absorb thin film. First, three broadband absorption peaks (3.2 THz, 4.7 THz, and 5.2 THz) are generated by localized VO_2 absorption, while the fourth (3.7 THz) broadband absorption is mainly caused by unit cell and ground plane interaction. On the other hand, it is found that the thickness of VO_2 and quartz has an effect on the absorber's absorption. In order to keep things short, we only explain the absorption analysis when the incidence is normal.

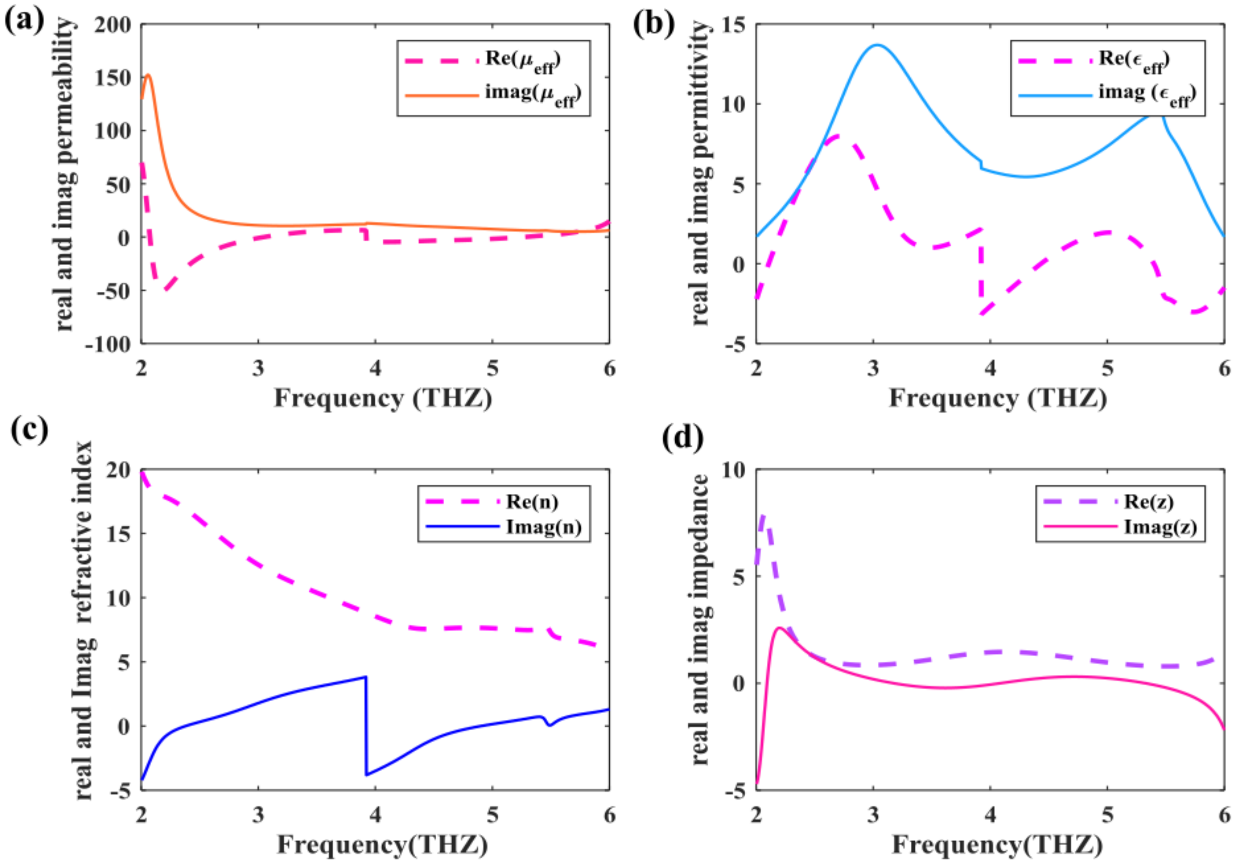

Figure 7. When $\sigma = 2 \times 10^5$ S/m, the effective physical parameters of (**a**) permittivity of the design structure, (**b**) permeability of the design structure, (**c**) refractive index of the design structure, and (**d**) impedance of the design absorber are obtained.

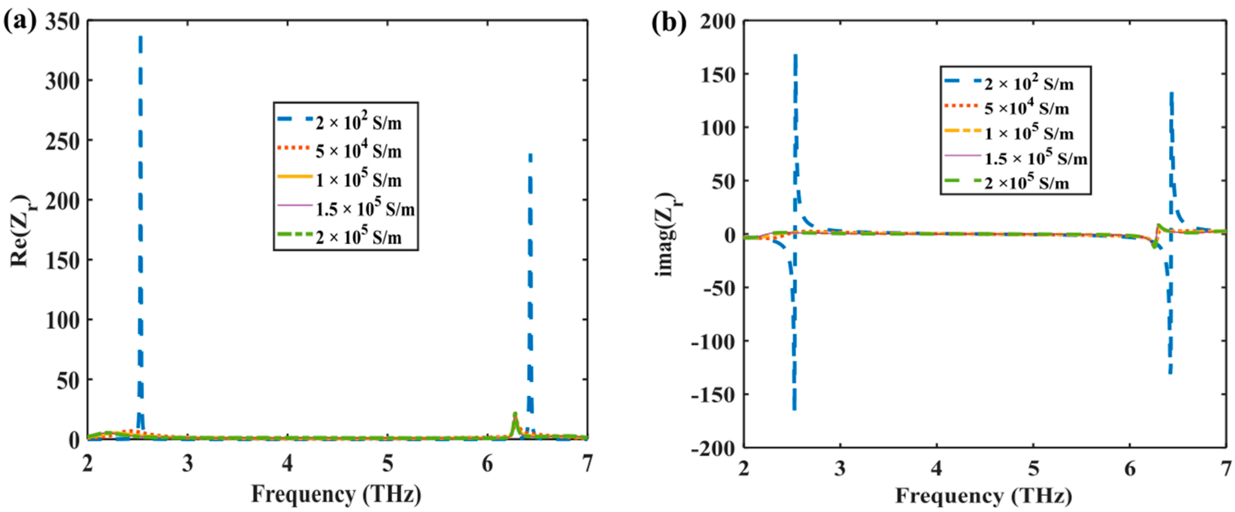

Figure 8. Simulation results (**a**) real part and (**b**) imaginary part of the relative impedance for VO_2 with various conductivities.

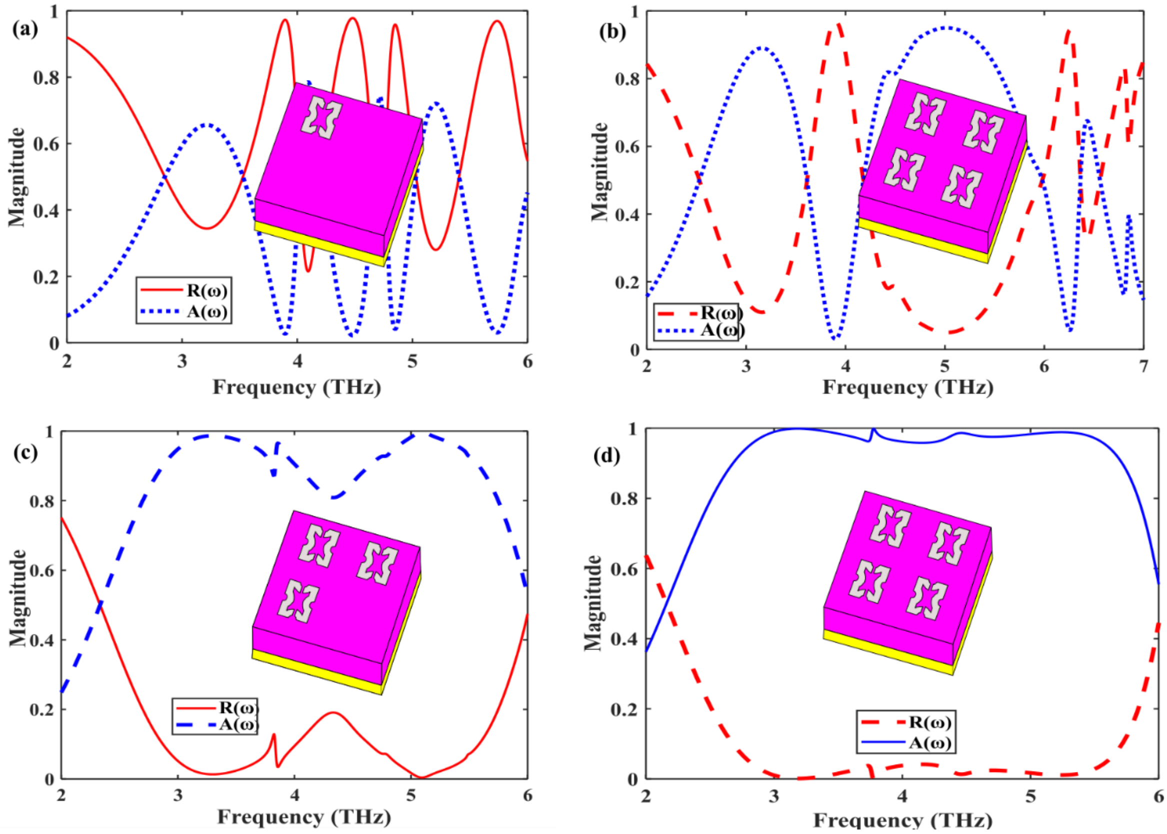

Figure 9. The structure's reflections and absorption bands (**a**) with a single arc-shaped VO_2 patch on top; (**b**) with a two-arc VO_2 pattern on top; (**c**) with a three-arc VO_2 pattern on top; (**d**) with four equal arc-shaped VO_2 patterns positioned diagonally on the top.

Absorption and thickness are shown in Figure 12a when the VO_2 conductivity is held constant at $\sigma = 2 \times 10^5$ S/m, as depicted in the figure. The computed data show that the recommended system's absorption is thickness-dependent under normal incidence. While absorption does not rise substantially if VO_2 thickness is less than 0.5 µm, when VO_2 thickness crosses this threshold, absorption increases and stabilizes because VO_2 is thick enough to impede the passage of energy.

When the thickness (h) of the dielectric layer (quartz) fluctuates from 6 µm to 12 µm in increments of 2 µm across a wide frequency range, the absorption of the proposed absorber increases. Between 2.7 and 5.7 THz, the dielectric layer's absorption must be greater than or equal to 90%, which is why its thickness (11 µm) was carefully chosen. In real-world applications, the effects of polarization and incidence angle on absorption performance must be considered. Figure 13 displays the absorption spectra for TE polarizations. As can be observed, when the polarization angle is altered from 0° to 45°, the proposed absorber's absorption spectra remain essentially unchanged. The absorption efficiency from 2.7 to 5.7 THz is still greater than 90% even when the incidence angle is up to 60°. Beyond 45°, the absorption and bandwidth, on the other hand, fall significantly. As the incident magnetic field's x component shrinks with increasing incident angle, the magnetic polarization cannot be stimulated as efficiently, and the absorber's ability to absorb energy is reduced. Thus, the proposed VO_2-based metamaterial absorber has excellent absorption capability for TE modes in the 45° angle range.

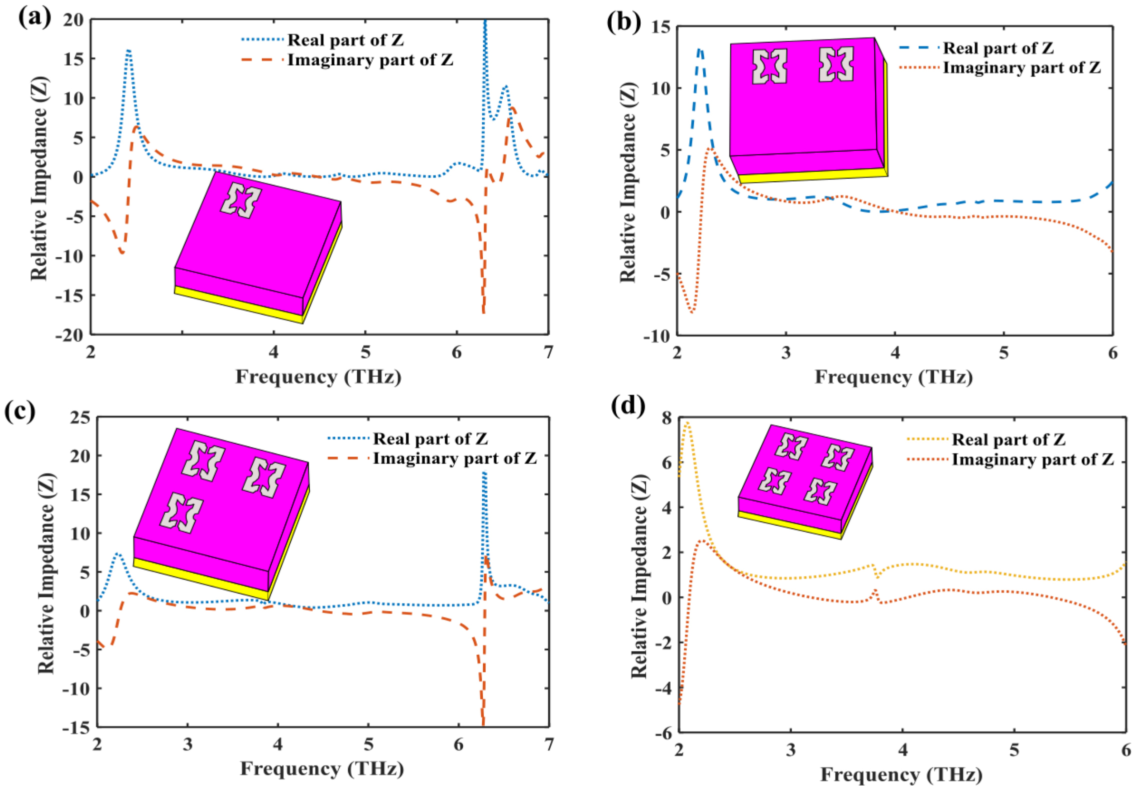

Figure 10. Relative impedance of the design steps (**a**) with a single arc-shaped VO_2 patch on top; (**b**) with a two-arc VO_2 pattern on top; (**c**) with a three-arc VO_2 pattern on top; (**d**) with four equal arc-shaped VO_2 patterns positioned diagonally on the top.

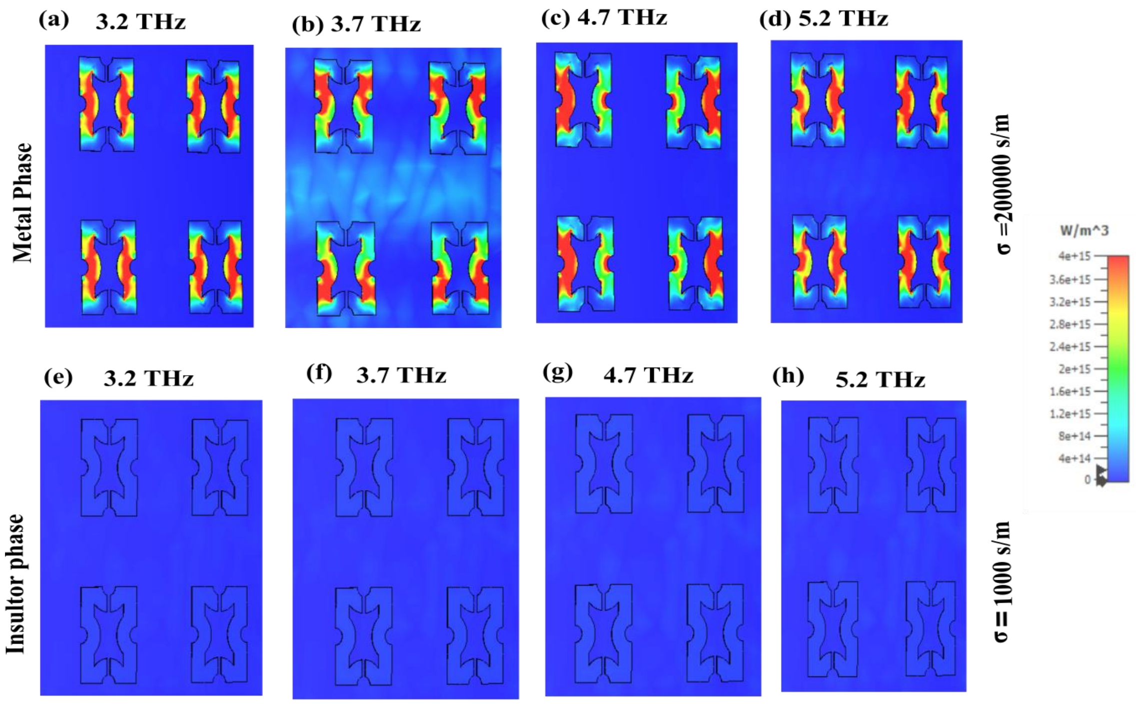

Figure 11. Simulated power loss density (PLD) at four (*f1*, *f2*, *f3*, *f4*) absorption peaks in the VO_2 layer (**a**–**d**) when conductivity is 2×10^5 S/m and when (**e**–**h**) VO_2 is in its insulator phase at conductivity of 1×10^3 S/m.

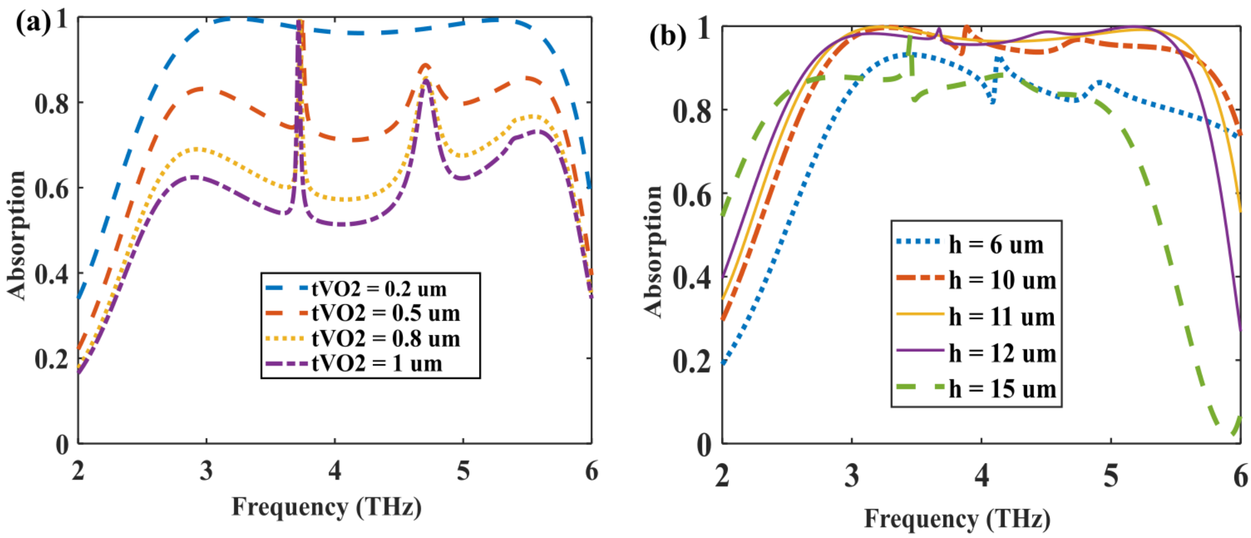

Figure 12. The influence of the (**a**) thickness of VO_2 and (**b**) thickness of the middle dielectric layer (quartz) on the design absorber absorption.

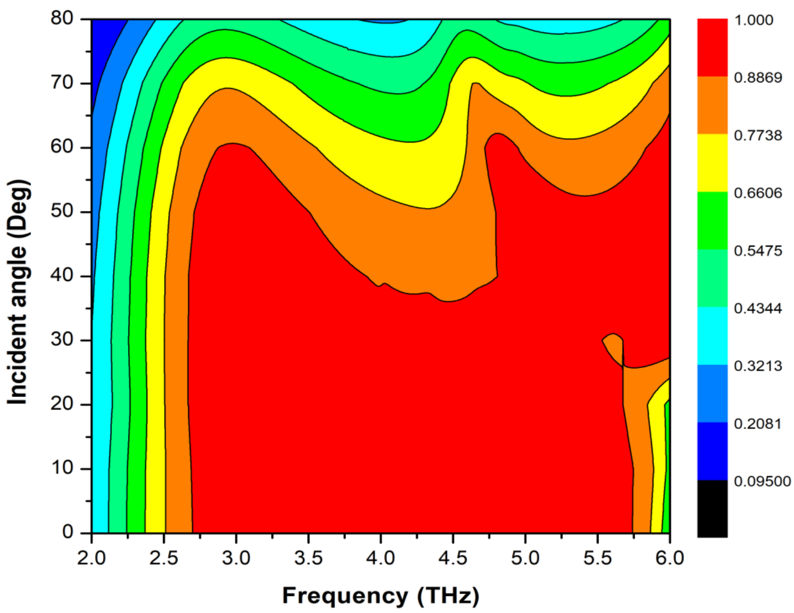

Figure 13. Incidence angle dependence of absorption phenomenon for TE polarization when $\sigma = 20 \times 10^4$ S/m.

5. Conclusions

In conclusion, we proposed a tunable ultra-wideband absorber composed of four identical arc-shaped structures made of phase transition material vanadium dioxide (VO_2). The proposed structure transforms from a reflector to an absorber by changing the conductivity from 200 S/m to 2×10^5 S/m and the absorbance at peak frequencies can be consistently tuned from 4% to 100%. Compared to previously reported VO_2-based absorbers, this absorption is significantly improved. Power loss density (PLD) and impedance-matching theory are further analyzed to learn more about the physical origin of ultra-wide absorption. This absorber is polarization-insensitive, and its absorption capability is constant up to 60° for TE polarization. This research may pave the way for developing terahertz metamaterial devices that are incredibly active and tunable. Numerous applications may be envisioned, including modulators, sensors, and dynamic filters.

Author Contributions: Conceptualization, U.U.R.Q. and M.I.K.; methodology, U.U.R.Q. and B.H.; software, U.U.R.Q.; validation, U.U.R.Q., M.I.K. and B.H.; formal analysis, U.U.R.Q. and M.I.K.; investigation, U.U.R.Q., M.I.K. and B.H.; resources, U.U.R.Q., M.I.K. and B.H.; data curation, U.U.R.Q.; writing—original draft preparation, U.U.R.Q.; writing—review and editing, U.U.R.Q., M.I.K. and B.H.; visualization, U.U.R.Q., M.I.K. and B.H.; supervision, M.I.K. and B.H.; project administration, U.U.R.Q.; funding acquisition, B.H. All authors have read and agreed to the published version of the manuscript.

Funding: This work was supported by the National Natural Science Foundation of China (No. 61875010).

Institutional Review Board Statement: Not applicable.

Informed Consent Statement: Not applicable.

Data Availability Statement: Not applicable.

Conflicts of Interest: The authors declare no conflict of interest.

References

1. Yang, G.; Yan, F.; Du, X.; Li, T.; Wang, W.; Lv, Y.; Hou, Y. Tunable broadband terahertz metamaterial absorber based on vanadium dioxide. *AIP Adv.* **2022**, *12*, 045219. [CrossRef]
2. Huang, K.C.; Wang, Z. Terahertz terabit wireless communication. *IEEE Microw. Mag.* **2011**, *12*, 108–116. [CrossRef]
3. Federici, J.F.; Schulkin, B.; Huang, F.; Gary, D.; Barat, R.; Oliveira, F.; Zimdars, D. THz imaging and sensing for security applications-explosives, weapons and drugs. *Semicond. Sci. Technol.* **2005**, *20*, S266–S280. [CrossRef]
4. Dean, P.; Mitrofanov, O.; Keeley, J.; Kundu, I.; Li, L.; Linfield, E.H.; Davies, A.G. Apertureless near-field terahertz imaging using the self-mixing effect in a quantum cascade laser. *Appl. Phys. Lett.* **2016**, *108*, 091113. [CrossRef]
5. Chiang, Y.; Yang, C.; Yang, Y.; Pan, C.; Yen, T. An ultrabroad terahertz bandpass filter. *Appl. Phys. Lett.* **2011**, *99*, 191909. [CrossRef]
6. Xiong, R.; Li, J. Double layer frequency selective surface for Terahertz bandpass filter. *J. Infrared Millim. Terahertz Waves* **2018**, *39*, 1039–1046.
7. Li, X.; Yang, L.; Hu, C.; Luo, X.; Hong, M. Tunable bandwidth of band-stop filter by metamaterial cell coupling in optical frequency. *Opt. Express* **2011**, *19*, 5283–5289. [CrossRef]
8. Cong, L.; Tan, S.; Yahiaoui, R.; Yan, F.; Zhang, W.; Singh, R. Experimental demonstration of ultrasensitive sensing with terahertz metamaterial absorbers: A comparison with the metasurfaces. *Appl. Phys. Lett.* **2015**, *106*, 031107. [CrossRef]
9. Arik, K.; AbdollahRamezani, S.; Khavasi, A. Polarization insensitive and broadband terahertz absorber using graphene disks. *Plasmonics* **2017**, *12*, 393–398. [CrossRef]
10. Alaee, R.; Farhat, M.; Rockstuhl, C.; Lede, F. A perfect absorber made of a graphene micro-ribbon metamaterial. *Opt. Express* **2012**, *20*, 28017–28024. [CrossRef]
11. Cong, L.; Cao, W.; Zhang, X.; Tian, Z.; Gu, J.; Singh, R.; Han, J.; Zhang, W. A perfect metamaterial polarization rotator. *Appl. Phys. Lett.* **2013**, *103*, 171107. [CrossRef]
12. Liu, X.; Tyler, T.; Starr, T.; Starr, A.F.; Jokerst, N.M.; Padilla, W.J. Taming the Blackbody with Infrared Metamaterials as Selective Thermal Emitters. *Phys. Rev. Lett.* **2011**, *107*, 045901. [CrossRef] [PubMed]
13. Alves, F.; Kearney, B.; Grbovic, D.; Karunasiri, G. Narrowband terahertz emitters using metamaterial films. *Opt. Express* **2012**, *20*, 21025–21032. [CrossRef] [PubMed]
14. Atwater, H.A.; Polman, A. Plasmonics for improved photovoltaic devices. *Nat. Mater.* **2010**, *9*, 205–213, Erratum in *Nat. Mater.* **2010**, *9*, 865. [CrossRef] [PubMed]
15. Wang, Y.; Sun, T.; Paudel, T.; Zhang, Y.; Ren, Z.; Kempa, K. Metamaterial-plasmonic absorber structure for high efficiency amorphous silicon solar cells. *Nano Lett.* **2012**, *12*, 440–445. [CrossRef] [PubMed]
16. Ni, X.; Wong, Z.J.; Mrejen, M.; Wang, Y.; Zhang, X. An ultrathin invisibility skin cloak for visible light. *Science* **2015**, *349*, 1310–1314. [CrossRef] [PubMed]
17. Schurig, D.; Mock, J.J.; Justice, B.J.; Cummer, S.A.; Pendry, J.B.; Starr, A.F.; Smith, D.R. Metamaterial electromagnetic cloak at microwave frequencies. *Science* **2006**, *314*, 977–980. [CrossRef] [PubMed]
18. Landy, N.I.; Sajuyigbe, S.; Mock, J.J.; Smith, D.R.; Padilla, W.J. Perfect metamaterial absorber. *Phys. Rev. Lett.* **2008**, *100*, 207402. [CrossRef]
19. Duan, G.; Schalch, J.; Zhao, X.; Zhang, J.; Averitt, R.D.; Zhang, X. Identifying the perfect absorption of metamaterial absorbers. *Phys. Rev. B* **2018**, *97*, 035128. [CrossRef]
20. Ma, Y.; Chen, Q.; Grant, J.; Saha, S.C.; Khalid, A.; Cumming, D.R. A terahertz polarization insensitive dual band metamaterial absorber. *Opt. Lett.* **2011**, *36*, 945–947. [CrossRef]
21. Shen, X.; Yang, Y.; Zang, Y.; Gu, J.; Han, J.; Zhang, W.; Cui, T.J. Triple-band terahertz metamaterial absorber: Design, experiment, and physical interpretation. *Appl. Phys. Lett.* **2012**, *101*, 154102. [CrossRef]
22. Hendrickson, J.; Guo, J.; Zhang, B.; Buchwald, W.; Soref, R. Wideband perfect light absorber at midwave infrared using multiplexed metal structures. *Opt. Lett.* **2012**, *37*, 371–373. [CrossRef] [PubMed]

23. Cheng, C.; Abbas, M.N.; Chiu, C.; Lai, K.; Shih, M.; Chang, Y. Wide-angle polarization independent infrared broadband absorbers based on metallic multi-sized disk arrays. *Opt. Lett.* **2012**, *20*, 10376–10381. [CrossRef]
24. Shan, Y.; Chen, L.; Shi, C.; Cheng, Z.; Zang, X.; Xu, B.; Zhu, Y. Ultrathin flexible dual band terahertz absorber. *Opt. Commun.* **2015**, *350*, 63–70. [CrossRef]
25. Liu, S.; Chen, H.; Cui, T.J. A broadband terahertz absorber using multi-layer stacked bars. *Appl. Phys. Lett.* **2015**, *106*, 151601. [CrossRef]
26. Li, W.; Wu, T.; Wang, W.; Guan, J.; Zhai, P. Integrating non-planar metamaterials with magnetic absorbing materials to yield ultra-broadband microwave hybrid absorbers. *Appl. Phys. Lett.* **2014**, *104*, 022903. [CrossRef]
27. Deng, H.; Stan, L.; Czaplewski, D.A.; Gao, J.; Yang, X. Broadband infrared absorbers with stacked double chromium ring resonators. *Opt. Express* **2017**, *25*, 28295–28304. [CrossRef]
28. Cheng, Y.; Gong, R.; Cheng, Z. A photoexcited broadband switchable metamaterial absorber with polarization insensitive and wide-angle absorption for terahertz waves. *Opt. Commun.* **2016**, *361*, 41–46. [CrossRef]
29. Jin, X.; Wang, F.; Huang, S.; Xie, Z.; Li, L.; Han, X.; Chen, H.; Zhou, H. Coherent perfect absorber with independently tunable frequency based on multilayer graphene. *Opt. Commun.* **2019**, *446*, 44–50. [CrossRef]
30. Shin, J.; Park, K.H.; Ryu, H.C. Electrically controllable terahertz square-loop metamaterial based on VO2 thin film. *Nanotechnology* **2016**, *27*, 195202. [CrossRef]
31. Wang, R.; Li, L.; Liu, J.; Yan, F.; Tian, F.; Tian, H.; Zhang, J. Weimin Sun Triple-band tunable perfect terahertz metamaterial absorber with liquid crystal. *Opt. Express* **2017**, *25*, 32280–32289. [CrossRef]
32. Hu, F.; Wang, H.; Zhang, X.; Xu, X.; Jiang, W.; Rong, Q.; Zhao, S.; Jiang, M.; Zhang, W.; Han, J. Electrically triggered tunable 400 terahertz band-pass filter based on VO2 hybrid metamaterial. *IEEE J. Sel. Top. Quantum Electron.* **2019**, *25*, 4700207. [CrossRef]
33. Li, Q.; Liu, S.; Zhang, X.; Wang, S.; Chen, T. Electromagnetically induced transparency in terahertz metasurface composed of meanderline and U-shaped resonators. *Opt. Express* **2020**, *28*, 8792–8801. [CrossRef]
34. Liu, L.; Kang, L.; Mayer, T.S.; Werner, D.H. Hybrid metamaterials for electrically triggered multifunctional control. *Nat. Commun.* **2016**, *7*, 13236. [CrossRef]
35. Wen, Q.; Zhang, H.; Yang, Q.; Xie, Y.; Chen, K.; Liu, Y. Terahertz metamaterials with VO2 cut-wires for thermal tunability. *Appl. Phys. Lett.* **2010**, *97*, 021111. [CrossRef]
36. Lappalainen, J.; Heinilehto, S.; Jantunen, H.; Lantto, V. Electrical and optical properties of metal-insulator-transition VO_2 thin films. *J. Electroceramics* **2009**, *22*, 73–77. [CrossRef]
37. Liu, J.; Fan, L. Development of a tunable terahertz absorber based on temperature control. *Microw. Opt. Technol. Lett.* **2020**, *62*, 1681–1685.
38. Choi, S.B.; Kyoung, J.S.; Kim, H.S.; Park, H.R.; Park, D.J.; Kim, B.J.; Ahn, Y.H.; Rotermund, F.; Kim, H.T.; Ahn, K.J.; et al. Nanopattern enabled terahertz all-optical switching on vanadium dioxide thin film. *Appl. Phys. Lett.* **2011**, *98*, 071105. [CrossRef]
39. Zhang, Y.; Qiao, S.; Sun, L.; Shi, Q.; Huang, W.; Li, L.; Yang, Z. Photoinduced active terahertz metamaterials with nanostructured vanadium dioxide film deposited by sol-gel method. *Opt. Express* **2014**, *22*, 11070–11078. [CrossRef]
40. Song, Z.; Wang, K.; Li, J.; Liu, Q.H. Broadband tunable terahertz absorber based on vanadium dioxide metamaterials. *Opt. Express* **2018**, *26*, 7148–7154. [CrossRef] [PubMed]
41. Wang, S.; Cai, C.; You, M.; Liu, F.; Wu, M.; Li, S.; Bao, H.; Kang, L.; Werner, D.H. Vanadium dioxide based broadband THz metamaterial absorbers with high tunability: Simulation study. *Opt. Express* **2019**, *27*, 19436–19447. [CrossRef]
42. Song, Z.; Wei, M.; Wang, Z.; Cai, G.; Liu, Y.; Zhou, Y. Terahertz absorber with reconfigurable bandwidth based on isotropic 421 vanadium dioxide metasurfaces. *IEEE Photon. J.* **2019**, *11*, 4600607. [CrossRef]
43. Bai, J.; Zhang, S.; Fan, F.; Wang, S.; Sun, X.; Miao, Y.; Chang, S. Tunable broadband THz absorber using vanadium dioxide metamaterials. *Opt. Commun.* **2019**, *452*, 292–295. [CrossRef]
44. Wang, T.; Zhang, Y.; Zhang, H.; Cao, M. Dual-controlled switchable broadband terahertz absorber based on a graphene-vanadium dioxide metamaterial. *Opt. Mater. Express* **2020**, *10*, 369. [CrossRef]
45. Dao, R.; Kong, X.; Zhang, H.; Su, X. A tunable broadband terahertz metamaterial absorber based on the vanadium dioxide. *Optik* **2019**, *180*, 619–625. [CrossRef]
46. Dong, X.; Luo, X.; Zhou, Y.; Lu, Y.; Hu, F.; Xu, X.; Li, G. Switchable broadband and wide-angular terahertz asymmetric transmission based on a hybrid metal-VO_2 metasurface. *Opt. Express* **2020**, *28*, 30675–30685. [CrossRef]
47. Dong, X.; Liu, C.; Huang, Y.; Hu, F.; Jin, Y.E.Y.; Zhou, Y.; Xu, X. Angular-dependent circular dichroism of tai chi chiral metamaterials in terahertz region. *Appl. Opt.* **2020**, *59*, 3686–3691. [CrossRef] [PubMed]
48. Liu, H.; Wong, L.; Wang, S.; Tang, S.; Zhang, X. Ultrafast insulator–metal phase transition in vanadium dioxide studied using optical pump–terahertz probe spectroscopy. *J. Phys. Condens. Matter* **2012**, *24*, 415604. [CrossRef]
49. Otto, M.R.; de Cotret, P.L.R.; Valverde-Chavez, D.A.; Tiwari, K.L.; Emond, N.; Chaker, M.; Cooke, D.G.; Siwick, B.J. How optical excitation controls the structure and properties of vanadium dioxide. *Proc. Natl. Acad. Sci. USA* **2019**, *116*, 450–455. [CrossRef] [PubMed]
50. Numan, A.B.; Mohammad, S.S. Extraction of material parameters for metamaterials using a full-wave simulator [education column]. *IEEE Antennas Propag. Mag.* **2013**, *55*, 202–211. [CrossRef]
51. Chen, X.; Grzegorcezyk, T.M.; Wu, B.; Pacheco, J., Jr. Kong Robust Method to Retrieve the Constitutive Effective Parameters of Metamaterials. *Phys. Rev. E* **2004**, *70*, 016608. [CrossRef] [PubMed]

52. Zhou, Z.; Song, S. Switchable bifunctional metamaterial for terahertz anomalous reflection and broadband absorption. *Phys. Scr.* **2021**, *96*, 115506. [CrossRef]
53. Huang, J.; Li, J.; Yang, Y.; Li, J.; Li, J.; Zhang, Y.; Yao, J. Broadband terahertz absorber with a flexible, reconfigurable performance based on hybrid-patterned vanadium dioxide metasurfaces. *Opt. Express* **2020**, *28*, 17832–17840. [CrossRef] [PubMed]
54. Abdulkarim, Y.I.; Awl, H.N.; Muhammadsharif, F.F.; Bakır, M.; Alkurt, F.Ö.; Altıntaş, O.; Dong, J.; Saeed, S.R.; Taouzari, M.; Karaaslan, M.; et al. A vanadium 446 dioxide-based metamaterial with quatrefoil and circle loaded structure on flexible polyamide substrate for terahertz applications. *Front. Phys.* **2022**, *10*, 968310. [CrossRef]
55. Xu, Z.; Ferraro, D.; Zaltron, A.; Galvanetto, N.; Martucci, A.; Sun, L.; Yang, P.; Zhang, Y.; Wang, Y.; Liu, Z.; et al. Optical detection of the susceptibility tensor in two-dimensional crystals. *Commun. Phys.* **2021**, *4*, 215. [CrossRef]